Velocity Observations in the West Passage of Narragansett Bay: A Partially Mixed Estuary

ROBERT H. WEISBERG

Graduate School of Oceanography, University of Rhode Island, Kingston 02881

WILTON STURGES

Department of Oceanography, The Florida State University, Tallahassee 32306

(Manuscript received 10 September 1975, in revised form 19 November 1975)

ABSTRACT

Narragansett Bay is a weakly stratified estuary comprised of three connecting passages of varying depths. The vertical distribution of horizontal velocity was observed in the West Passage using moored current meters. The instantaneous motion was characterized by semi-diurnal tidal currents of amplitude 25–60 cm s^{-1}. These currents exhibited a phase advance with depth (total water depth = 12.8 m) ranging with lunar phase from 0–3 h. The net current time series obtained by filtering out motions at tidal and higher frequencies were found to be an order of magnitude less than the instantaneous motion and well correlated to the prevailing 2–10 m s^{-1} winds. For periodicities of 2–3 days, the coherence between the longitudinal components of wind and net near surface current was as high as 0.8 with the current lagging the wind by about 3 h. The mean near surface speed, obtained by averaging over one month, was 1.2 ± 1.6 cm s^{-1}. The large error bounds were a result of the large variability of the net current time series (and *not* a result of inadequate sampling). A measure of this variability due to day-to-day changes in weather is given by the root mean square deviation of the net current time series or 2.6 cm s^{-1}. The net transport of water through the West Passage was observed to be seaward or landward over the entire water column for several days duration, with typical wind induced transport fluctuations of ± 500 m^3 s^{-1}. Hence, a net communication of water exists between the East and West Passages with water flowing either way in response to the wind. Wind is concluded to be the dominant mechanism driving the net circulation in the West Passage of Narragansett Bay. This is in contrast with the classical views of gravitationally convected net estuarine circulation.

1. Introduction

Narragansett Bay is a partially mixed estuary. It consists of three connecting passages, as shown in Fig. 1, each of different depth and configuration. This paper examines the net circulation, or time-averaged motions at sub-tidal frequencies, and transport in the West Passage of Narragansett Bay. The West Passage has a vertical salinity stratification of roughly 2‰ over 12 m. A general hydrographic description of the bay is given in Hicks (1959, 1963).

The published estuarine literature has been heavily weighted toward the gravitationally convected, or mean, portion of estuarine circulation. Based upon the constraints of water and salt conservation in the mean state, several schemes have been proposed for estimating this portion of the flow using rudimentary measurements of salinity and velocity (e.g., Pritchard and Kent, 1956; Rattray and Hansen, 1962; Hansen and Rattray, 1966). These constraints cannot be simply applied in the West Passage since communication of water between the East and West Passages north of Conanicut Island may result in an unknown source or sink of both water and salt. Therefore, a direct sampling program was required. Direct velocity sampling over about 39 days was quite fruitful since it clearly demonstrated the importance of wind as a driving mechanism for net estuarine circulation. This finding is qualitatively attuned with the implications of Hansen and Rattray's (1965) theoretical treatment of steady-state estuarine circulation and to short-term observations by Pickard and Rodgers (1959) in the Knight Inlet, British Columbia.

2. Field program

Current velocity measurements were obtained from two stations in the West Passage: one near Rome Point and one near Bonnet Shores (see Fig. 1). Both were near the deepest part of the passage and away from topographic irregularities. A total of eight Geodyne model A 100-SE current meters were installed during the fall of 1970. Six were uniformly distributed in the vertical at the Rome Point station on the rigid mooring shown in Fig. 2, and two were buoyantly suspended at the Bonnet Shores station as shown in Fig. 3. The use

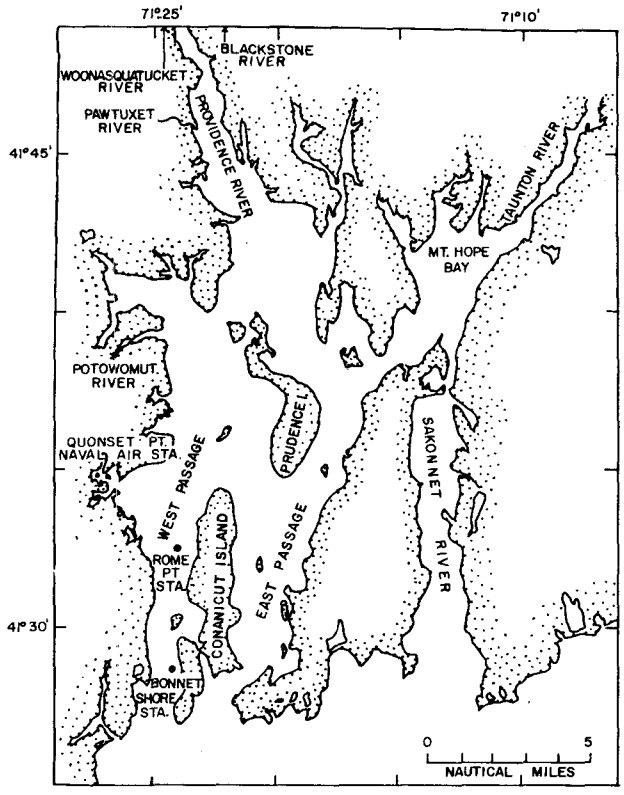

FIG. 1. A map of Narragansett Bay showing the station locations and principal rivers.

of two different mooring systems provided an independent check against biases due to mooring motion. Four Geodyne model 850 current meters were rigidly mounted at the Rome Point station during the spring of 1971. Table 1 lists the location, data number, and sampling duration for all of the useful data returns.

Both of the current meter types sensed speed with a Savonius rotor. They differed only in their recording scheme. The output from the photographic recording model A 100-SE current meters consisted of a speed and direction derived by scalar averaging over a 2.5 min sampling burst. The magnetic cartridge recording model 850 current meters resulted in a speed and direction every 7.5 min derived by vector averaging over a 2.5 min sample burst.

Hourly values of wind speed and direction were obtained from the U. S. Naval Air Station at Quonset Point, R. I. (Fig. 1). For a more detailed data report including measurements of the vertical and longitudinal salinity and density gradients, reference is made to Weisberg and Sturges (1973).

3. The data

Though the primary intent of this paper is to view the net motions, some interesting aspects of the instantaneous currents also warrant discussion. The longitudinal axis of the West Passage is oriented in the north–south direction, so only north components will be presented herein; the east components were relatively very small with fluctuations only at tidal and higher frequencies.

a. Tidal oscillations

The currents in the West Passage are dominated by semi-diurnal tidal oscillations ranging in amplitude between about 25 cm s^{-1} at neap tides to about 60 cm s^{-1} at spring tides. Fig. 4 shows the kinetic energy density spectrum for the north component of near surface current (GSO-64). The spectrum was computed with 10 degrees of freedom. Prominent peaks occur at diurnal, semi-diurnal (M_2), and quarter-diurnal (M_4) tidal frequencies. Smaller peaks also appear at the M_6 tidal harmonic and at sub-tidal frequencies.

The general character of the observed waveforms during neap and spring tides is shown in Fig. 5. Overplotted are hourly vector-averaged north components separated in the vertical by 5.1 m (GSO-64 and GSO-61). The current strength during ebb tends to be stronger than during flood; however, the flood is longer lasting due to an inflection point (the double flood, as it is commonly called). The harmonic structure varies from neaps to springs. Table 2 lists the root mean square (rms) current speed, the partition of energy into the M_2 and M_4 tidal constituents, and the phase

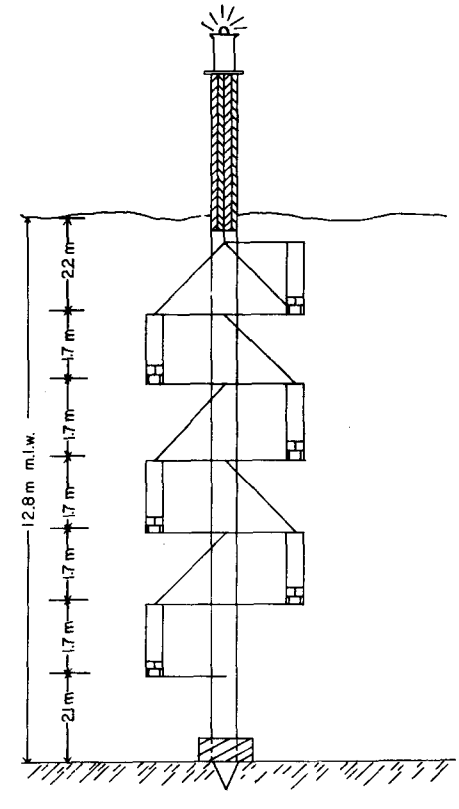

FIG. 2. The rigidly moored array used at the Rome Point station.

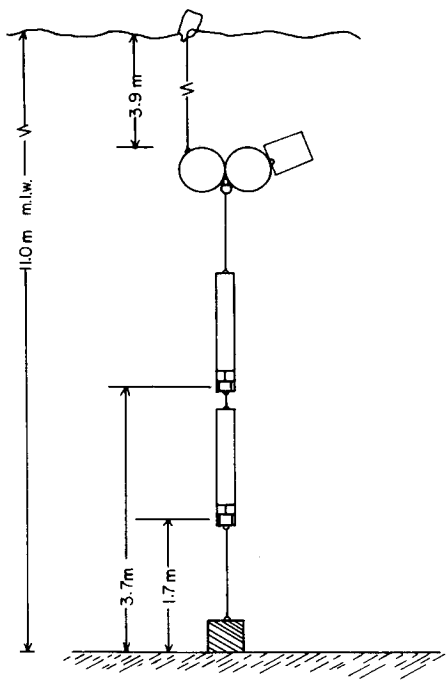

FIG. 3. The buoyantly moored array used at the Bonnet Shores station.

difference between the M_2 constituents at two different depths for two 50 h pieces of record GSO-64: one at neap tide and one at spring tide. The waveforms at neap tide are more complex than at spring tide as evidenced by the percentage of energy contained in the two principal tidal frequencies. During spring tides the M_2 and M_2+M_4 frequencies contain as much as 89% and 97% of the tidal kinetic energy, as opposed to as little as 76% and 80% during neap tides.

Along with the harmonic distortion of the semi-diurnal tidal signal, the most conspicuous feature of Fig. 5 is the phase difference between the currents measured at the depths of 2.1 and 7.2 m. The deeper currents lead the near surface currents throughout the record. Cannon (1969) observed a similar phenomenon in the Patuxent estuary and he discussed it in terms of Proudman's (1953) analysis of bottom friction effects. Here the phenomenon is more complicated. As observed by eye, the phase advance appears to be asymmetric about a tidal cycle varying from near zero at spring tides to as much as 3 h during neap and intermediate range tides. The phase advance manifests itself in the instantaneous velocity profile as shown in Fig. 6 in which speed is plotted as a function of depth over the progression of a tidal cycle. At any instant in time the magnitude and direction of the flow may vary in the vertical. It is even possible to measure a seaward flow near the surface and a landward flow at depth. This, of course, should not be confused with the gravitational convection scheme of steady-state estuarine circulation. Further discussion of the phase advance will be given in a later section.

TABLE 1. The locations, data numbers, and sampling duration for all of the current meters yielding useful data.

Distance from the bottom (m)	Data no.	Sampling duration
	Rome Point Station*	
10.6	GSO-64	19 Oct–27 Nov 1970
8.9	GSO-63	19 Oct-19 Nov 1970
5.5	GSO-61	19 Oct–24 Nov 1970
3.8	GSO-60	19 Oct–5 Nov 1970
10.6	GSO-83	19 Mar–1 Apr 1971
3.8	GSO-81	17 Mar–1 Apr 1971
2.1	GSO-80	17 Mar–1 Apr 1971
	Bonnet Shores Station**	
3.7	GSO-65	29 Oct–7 Dec 1970
1.7	GSO 66	29 Oct–7 Dec 1970

* Location: 41°32′27″N, 71°24′54″W, depth (m.l.w.) = 12.8 m.
** Location: 41°28′40″N, 71°24′09″W, depth (m.l.w.) = 11.0 m.

b. *Net motion*

All of the current and wind velocity time series were low-pass filtered to remove the semi-diurnal and higher frequencies using a Gaussian-shaped filter having a width of 49 h and a standard deviation of 8 h. The half-amplitude response of this filter is somewhat less than 2 days.

The filtered time series from the fall 1970 experiment are shown in Fig. 7. The sign convention used for the

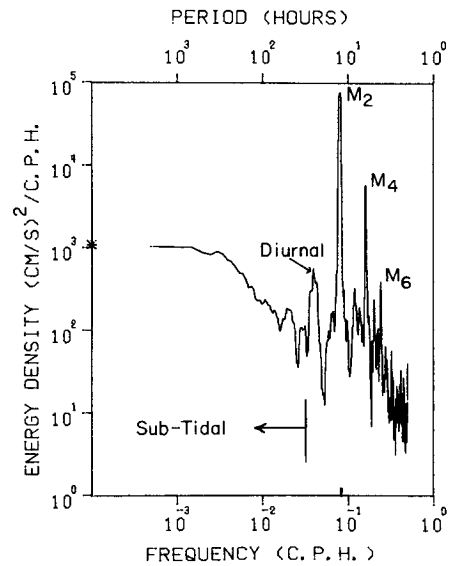

FIG. 4. A kinetic energy density spectrum for the north component of near-surface current (GSO-64). The computation has 10 degrees of freedom; error bars, however, are not shown since the majority of the signal is deterministic (the tides).

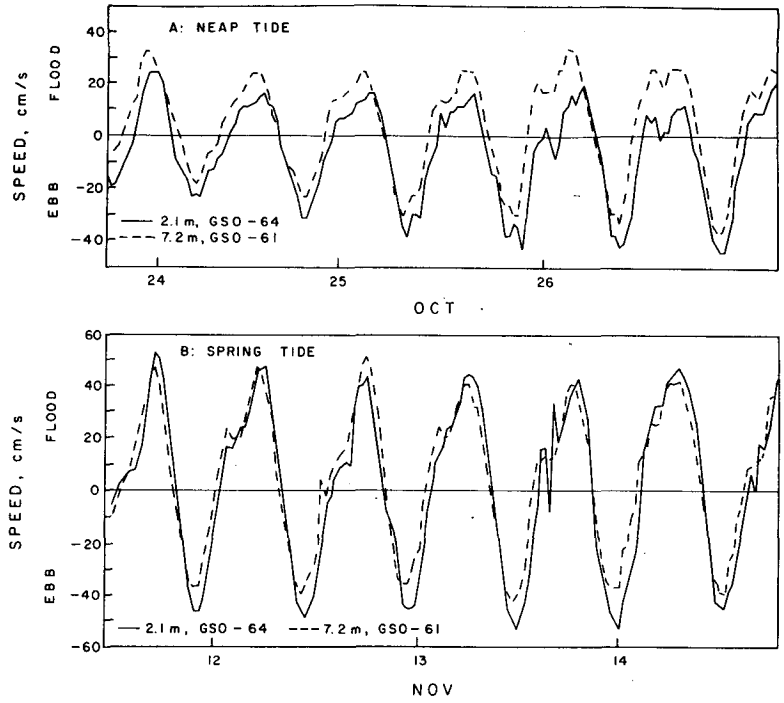

FIG. 5. The north component of velocity measured 2.1 m (full lines) and 7.2 m (dashed lines) below the surface during periods of neap and spring tide.

wind is opposite the meteorological convention, i.e., here a north wind blows *toward* the north. Note the exclusion of data on three occasions: 26–27 October, 2–3 November and 13–15 November, during which times the current meter data were likely to be badly contaminated by surface wave motions.[1]

TABLE 2. The rms north component of current speed, percentage of energy contained in the M_2 and M_4 tidal frequencies, and the phase difference for the M_2 constituent ($\Delta\phi$) between the two levels 2.1 m and 7.1 m below the surface. Values are listed for a neap and a spring tide.

	Neap tide (23–25 Oct)			Spring tide (11–13 Nov)		
Depth (m)	r.m.s. (cm s^{-1})	Percent M_2	Percent M_4	r.m.s. (cm s^{-1})	Percent M_2	Percent M_4
2.1	18.3	76	4	31.4	89	8
7.2	17.1	87	4	26.9	86	6
		$\Delta\phi$ (rad)				
2.1–7.2		0.16			0.23	

The mean values and rms deviations about the mean for the north component time series of current and wind velocity are given in Table 3. In terms of rms values the net currents are an order of magnitude less than the instantaneous currents. The mean values imply a flow reversal at mid-depth which is characteristic of gravitational convection with a seaward upper layer outflow and a landward lower layer inflow. Our observed means, however, are only estimates of the true means obtainable from much longer records. A measure of the variability, and hence the uncertainty, of the mean value estimates may be calculated by integrating the autocovariance function of the time series over all lags (e.g., Sturges, 1974). Assuming a normal probability distribution, the 95% confidence interval for the mean near surface current GSO-64 computed in

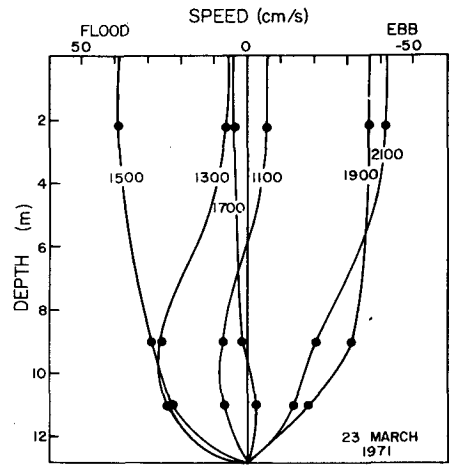

FIG. 6. The north component of velocity as a function of depth for various stages of a single tidal cycle at the Rome Point station.

[1] A Savonius rotor behaves nonlinearly to high-frequency forcing and the resulting rectification is impossible to correct for. Our error analysis (Weisberg and Sturges, 1973) suggested that the excluded data were unreliable. All of the data shown, however, are estimated as being precise to ± 0.5 cm s^{-1}.

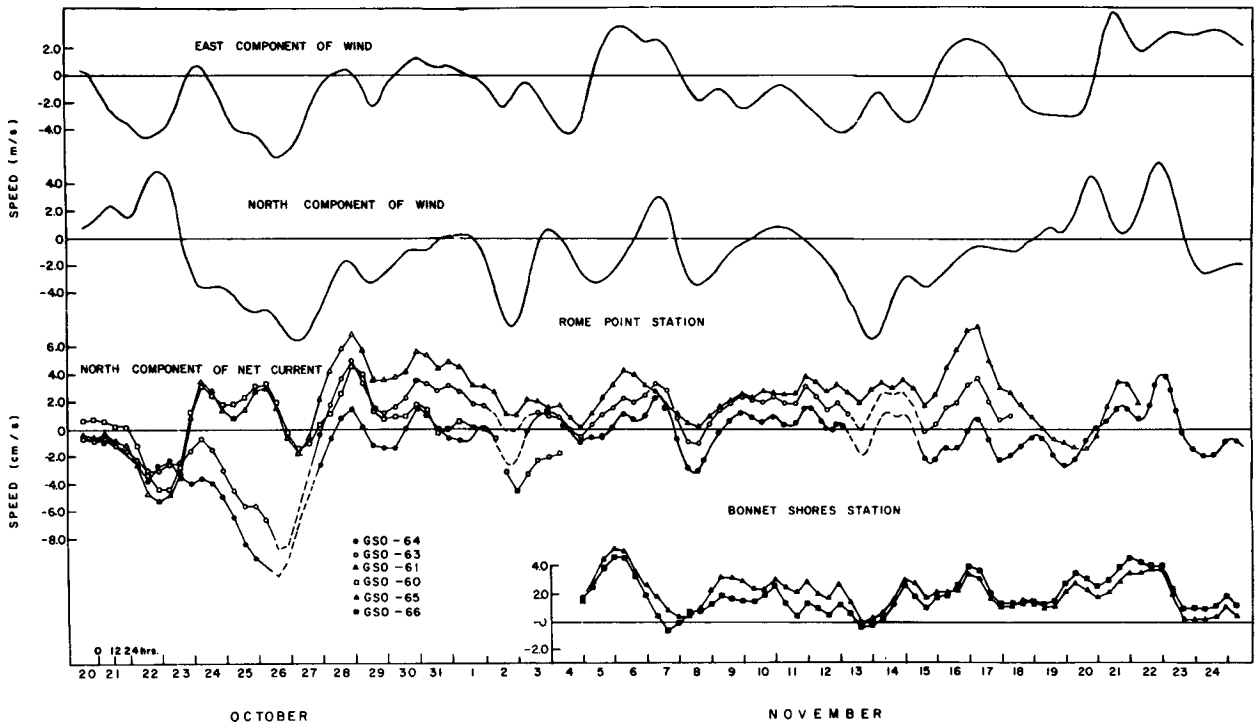

FIG. 7. The low-pass filtered wind and current velocity time series from the fall 1970 experiment (a northward wind is directed toward the north, etc.).

this manner is

$$\bar{u} = -1.2 \pm 1.6 \text{ cm s}^{-1}.$$

The point to be made here is that even with a record length of about one month, the variance of the mean estimate is large in comparison with the small mean estimate itself, thus making the statistical sense of the mean flow uncertain. Therefore, in viewing Fig. 7, attention should be focused upon the variability of the net currents and their correlation with the wind. Neither of these two features are prevalent in published estuarine literature.

The correlation between the low-pass filtered wind and current velocities is strongest for the north components which corresponds to the orientation of the channel and the direction of maximum fetch. A computation of coherence and phase between the north components of current and wind velocity showed a band of high coherence (~0.8) for time scales of from 2–3 days with the current lagging the wind by about 3 h. Assignment of confidence limits to the coherence and phase estimates in the usual manner is perhaps unwarranted due to the non-stationary nature of the

TABLE 3. The mean values and rms deviations about the mean for the observed and low-pass filtered north components of current from the fall 1970 for the Rome Point station and the north component of wind.

Data no.	Distance from the bottom (m)	Mean (cm s^{-1})	Root mean quare deviations: Low-passed (cm s^{-1})	Root mean quare deviations: Instantaneous (cm s^{-1})
GSO-64	10.6	−1.2	2.6	22.0
GSO-63	8.9	0.4	2.7	22.8
GSO-61	5.5	2.1	2.4	21.2
GSO-60	3.8	0.1	2.2	17.0
Wind		−1.2 m s^{-1}	3.2 m s^{-1}	3.6 m s^{-1}

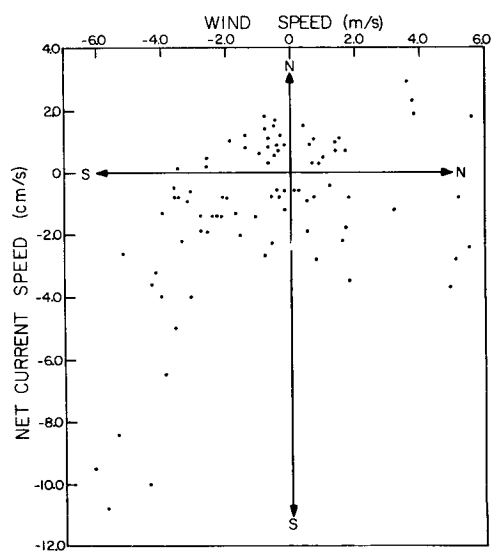

FIG. 8. A scatter plot showing the correlation between the north components of net near-surface current (GSO-64) and wind (a northward wind is directed toward the north, etc.).

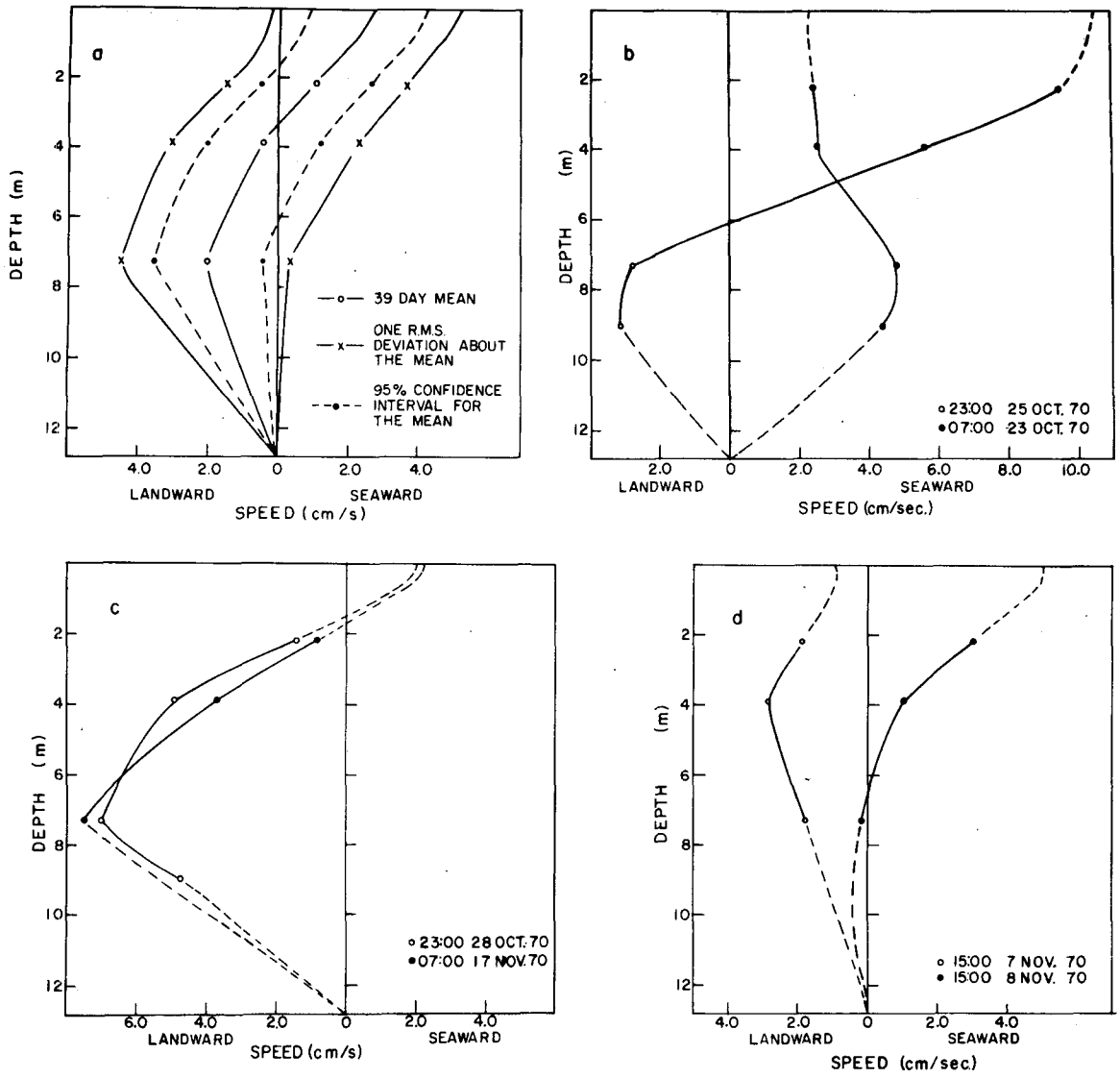

FIG. 9. Vertical profiles of the net north component of velocity for the mean estimates and for various wind conditions.

time series and the data gaps. Visual inspection of Fig. 7 also shows that the net currents were coherent vertically at both stations as well as longitudinally between them (with a longitudinal separation of 7 km).

A simple and informative way of viewing the wind/current correlation is by use of a scatter plot (Fig. 8), since a qualitative explanation can be afforded to each quadrant. The points were plotted at the filtering interval of 8 h. Quadrants one and three (the upper right and lower left) represent a positive correlation between the north components of wind and net near surface current; that is, northward blowing winds tend to produce northerly net currents and vice versa. In the absence of wind, we would expect the flow to be southerly. The points in quadrant four (lower right) are the result of winds blowing toward the northwest. This direction is perpendicular to the cross-sectional area joining the East and West Passages between Conanicut and Prudence Islands (see Fig. 1). Therefore, fourth-quadrant points are representative of wind-induced flow from the East to the West Passage. The resulting flow in the West Passage is south (seaward) by continuity. Most of the second-quadrant points (upper left) resulted after the sudden arrest of a strong southward wind. When a wind blows over a confined body of water, the surface and isopycnals slope to balance the stress of the wind. Upon removal of the wind stress, water must flow in the opposite direction for the slopes to relax. Hence, second-quadrant points represent a northward flux of water after subsidence of a strong southward blowing wind.

Vertical profiles of the net north velocity component are shown in Fig. 9 for the mean state (Table 2) and the situations described for the scatter plot. Plotted on

the mean state diagram (Fig. 9a) are the mean profile (solid line), the 95% confidence interval for the mean profile (dotted line), and the rms deviation of the net current time series about the mean. As already mentioned, the mean profile is indicative of two-layered flow, but even the direction of the flow is not statistically reliable. The most important aspect of this figure is the profiles of the mean plus or minus rms deviation. These suggest that in response to typical everyday fluctuations in weather, the net flow may be either seaward or landward over the *entire* water column. The implication of this finding should be clear, especially in the case of sampling programs which depend crucially on measurements over a few tidal cycles. An example of this is a dye diffusion experiment in which advection and diffusion of dye is studied over periods which might be shorter than that of the dominant motions.

Fig. 9b shows two contrasting cases, one for strong winds toward the southwest and one for strong winds toward the northwest. The former case results in two-layered flow with the upper layer speed greatly enhanced. The latter case results in a transport of water from the East to the West Passage. The flow near the surface, although south, is impeded by the wind relative to the larger speeds in the deeper waters.

Two independent relaxation events are shown in Fig. 9c. Prior to both events the wind had been blowing to the south, hence driving water out of the West Passage. A rapid abatement of the wind resulted in an influx of water. The strongest flow is at mid-depth and is consistent with the relaxation of isopycnal surfaces. Although the two events occurred about three weeks apart, they are almost identical.

Fig. 9d shows how quickly the West Passage responds to a change in wind direction. Within a day the entire net current distribution shifted from northerly to southerly flow in response to wind.

As an estimate of the net transports of water through the West Passage at the Rome Point station for the flow situations just discussed, the speeds shown in Fig. 9 may be numerically integrated over a cross-sectional area assuming lateral homogeneity. The results are given in Table 4. Three values are given for the transports. The upper and lower layer values refer to flow above and below the zero speed point; the total is the sum of the upper and lower layers. Since the zero speed point is variable, so are the definitions of the upper and lower layers. In some situations layering does not exist, i.e., flow is entirely north to south, so only the total transport value is given. Also shown in the table is the corresponding fresh water input to the West Passage. The error bounds on the net transport were calculated using the error bounds on the net speeds (± 0.5 cm s^{-1}) and do not include the possibility of lateral variability in the flow field. Drogue measurements of Kowalski *et al.* (1971) suggested lateral uniformity to within approximately 20%. Since the Rome Point station was situated near the deepest part of the West Passage, lateral variability would tend to decrease the net transport. Hence, the estimates given in Table 3 may be considered to be upper limits of the actual net transport.

TABLE 4. The net transport of water through the West Passage of Narragansett Bay estimated from the fall 1970 Rome Point station data. Estimates are given for the mean, the mean ± 1 rms deviation, and for various wind conditions. An asterisk denotes values that are not statistically different from zero. The average fresh water input rate to the West Passage during the experiment is included for comparison. Values are in m^3 s^{-1}.

Condition & Time	Transport: Upper layer	Transport: Lower layer	Transport: Total
Mean	−150*	110*	−40*
Mean +1 rms deviation			−540
Mean −1 rms deviation			460
Strong wind from SE			
0700, 23 Oct 1970			−60±100
Strong wind from NE			
1500, 26 Oct 1970	−1160±80	90±20	−1050±100
Relaxation			
2300, 28 Oct 1970	−50±20	660±80	610±100
0700, 17 Nov 1970	−50±20	580±80	530±100
Reversal			
1500, 7 Nov 1970			390±100
1500, 8 Nov 1970	−400±80	10±10	−390±100
Fresh water input			−5

The results of the spring experiment were qualitatively similar to those which have been presented. The net near-bottom currents varied from 3–7 cm s^{-1} and were always directed landward. The constant sense of the flow was probably caused by the order of magnitude increase in river input during the spring. Unfortunately, the near-surface record was too short and subject to too much wind-wave biasing to allow a meaningful computation of net flow. At one time after the subsidence of a strong southward wind, however, a relaxation event similar to those of the fall was observed.

4. Discussion

a. *Wind-induced transport*

As shown in Table 4, the net transport of water through the West Passage rarely, if ever, equals its river input. Rather, the net transport may be directed seaward or landward over the entire water column in response to the wind. Sustained transports of this fashion require either a large storage capacity or a source and sink.

Wind-induced water transport within an estuary results in a surface slope whose associated pressure gradient acts to balance the wind stress upon the sea surface. Neglecting bottom friction, the linearized steady-state surface slope in the presence of longitudinally uniform stratification is given by

$$\beta = \frac{\tau}{\rho g h} - \frac{1}{\rho}\frac{\partial \rho}{\partial x}\frac{h}{2}, \qquad (1)$$

where τ is the wind stress, ρ the density of the water at the surface, h the total depth, g the acceleration of gravity, and $\partial\rho/\partial x$ the longitudinal density gradient assumed uniform with depth. For a rectangular basin of length L the characteristic time t to set up the required slope is

$$t=\frac{\beta L^2}{2vh}, \tag{2}$$

where v is the vertically averaged longitudinal velocity component induced by the wind. Putting in the appropriate numbers for the West Passage it is estimated that, once the water column has been set into motion, it takes but an hour or so to redistribute enough water to balance the stress of a 5–10 m s^{-1} wind. Therefore, we might expect to find a net transport over the entire water column for a few hours, of sufficient volume to establish a new surface slope. However, the observations show that a net influx or efflux may occur for a few days. We conclude that under such conditions there must be a net communication of water between the East and West Passages.

The flow from the West Passage to the East Passage under the influence of a northward wind may easily be explained by the difference in the depths of the two passages. West Passage is only about two-thirds as deep as the East Passage. Since the surface slope is inversely proportional to depth, the water in the West Passage is raised a few centimeters higher than in the East Passage, resulting in a west-to-east pressure gradient.

b. *The phase advance of the instantaneous motion with depth*

How well does bottom friction account for the observed phase advance with depth of the instantaneous motion? Assuming a homogeneous fluid of constant eddy viscosity A, the linearized longitudinal equation of motion may be written

$$\frac{\partial u}{\partial t}-A\frac{\partial^2 u}{\partial z^2}=F\exp(i\omega t), \tag{3}$$

where z is the vertical coordinate (positive upward from the bottom) and u (z,t) is the tidal current as a function of depth and time. The forcing term on the right, for a shallow water tidal wave, is uniform with depth, and the angular frequency ω is taken to be the semi-diurnal tidal frequency. A tidal current reaches its maximum value when $\partial u/\partial t=0$. This occurs when the pressure gradient force is balanced by friction. The former is constant with depth, while the latter has a maximum at the bottom and decreases upward. Hence, $\partial u/\partial t=0$ first near the bottom and progressively later upward from the bottom. It intuitively follows that near-bottom currents lead near-surface currents.

Subject to the boundary conditions

$$\left.\begin{aligned} &u=0 \text{ at } z=0 \text{ (no slip)}\\ &\partial u/\partial z=0 \text{ at } z=0 \text{ (no shear stress at the surface)}\end{aligned}\right\},$$

a solution to the governing equation of motion (e.g., Lamb, 1932, pp. 622–623) is

$$u(z,t)=\frac{F}{\omega}\sin\omega t-\frac{F}{\omega}\exp(-\xi z)\sin(\omega t-\xi z), \tag{4}$$

where $\xi=(\omega/2A)^{\frac{1}{2}}$. The vertical extent of the frictional disturbance (the second term on the right) may be chosen as the point where $e^{-\xi z}=e^{-\pi}$ or $z=\pi/\xi$. Hence, the vertical extent depends upon the frequency of the motion and the eddy exchange of momentum. As an example, using 4 cm^2 s^{-1} as a value for the eddy viscosity [this value was estimated for the James River estuary by Rattray and Hansen, 1962)], the vertical extent of bottom frictional effects for the semi-diurnal tide is 7.5 m. It is evident that bottom friction may permeate most of the water column in a shallow estuary.

In order to examine the depth dependence of the amplitude and phase of the oscillatory current, we consider the solution in the alternative form

$$u(z,t)=B(z)\sin[\omega t-\alpha(z)], \tag{5}$$

where the amplitude function

$$B(z)=u_0[1-2\exp(-\xi z)\cos\xi z+\exp(-2\xi z)] \tag{6}$$

and the phase function

$$\alpha(z)=\tan^{-1}\left(\frac{-\sin\xi z}{\exp\xi z-\cos\xi z}\right). \tag{7}$$

$B(z)$ and $\alpha(z)$ are shown in Fig. 10 for various values of an assumed constant eddy viscosity. The limit of $\alpha(z)$ as z approaches zero (the bottom) is 45°, or about 1.5 h for the case of the semi-diurnal tide (M_2). Three sets of M_2 tidal constituent data are included in the figure. They were all obtained from Fourier decompositions over four tidal cycles. One set was taken from Cannon (1969) for the Patuxent estuary. The other two represent neap and spring tide conditions for our data. Plotted for the amplitude function are surface normalized rms speeds, and plotted for the phase function are the phase differences for the M_2 constituent between the surface and the particular depth. The observations agree fairly well with Eqs. (6) and (7), suggesting that the parameterization of bottom stress in this manner is useful. Note that our data shifts toward a larger value of eddy viscosity from neap to spring tides (~8–12 cm^2 s^{-1}) as expected for an increase in current strength.

Although this simple frictional model seems to account for the M_2 constituent alone, a separate explanation must be invoked to explain the behavior of the tidal signal as a whole, for which the phase advance is asymmetric about a tidal cycle and varies from 1–3 h

during neap and intermediate range tides to near zero during spring tides—as interpreted from zero crossings. The larger discrepancies about neap tides arise from the distortions in the waveform caused by the M_4 and higher tidal harmonics. Table 2 shows that these become relatively more energetic at neap tides and small changes in the amplitude ratio, or phase, between the M_4 and M_2 constituents have a large effect upon zero crossings (e.g., see U.S.C.G.S. Spec. Publ. No. 260, p. 36).

5. Summary

The instantaneous and net, or time-averaged, current structures at two locations in the West Passage of Narragansett Bay have been studied via direct current meter observations. Semi-diurnal tidal oscillations of amplitude varying between 25–60 cm s^{-1} from neap to spring tides dominated the instantaneous motion. The relative phase of the tidal oscillations advanced by as much as 3 h with depth. The amplitude of the net motion was an order of magnitude less and well correlated with the prevailing 2–10 m s^{-1} winds. The strongest correlation occurred between the north components (parallel to the longitudinal axis of the West Passage) of wind and near-surface net current velocities. The net currents were coherent vertically over the entire water column (12.5 m) as well as longitudinally between both stations (7 km separation). Hence, the West Passage seems to respond very well to the wind as a generating mechanism for net circulation over time scales on the order of a few days.

Net water transport calculations were made for various wind conditions. The net transport may be directed either seaward or landward over the entire water column for durations of a few days in response to wind. Typical wind-induced transport fluctuations are ± 500 m^3 s^{-1}. We conclude that a net flux of water must exist between the East and West Passages, the direction of this flow being wind-dependent.

In order to investigate gravitationally convected circulation apart from wind effects, averages were formed over the entire record length of one month. The resulting means had a two-layered structure with seaward flow in the upper layer and landward flow in the lower layer. However, the large variance and nonstationary nature of the net current time series make the statistical sense of the mean flow uncertain. Furthermore, it is doubtful whether gravitationally convected flow in the West Passage can be extracted from velocity observations irrespective of record length. This finding should not be nearly as severe in a single-channel estuary where continuity constrains the net transport to equal the river input. A mean flow estimate can be representative of gravitational convection in that case; but, only if the averaging interval is significantly larger than the periods of local wind fluctuations, even if the winds are light.

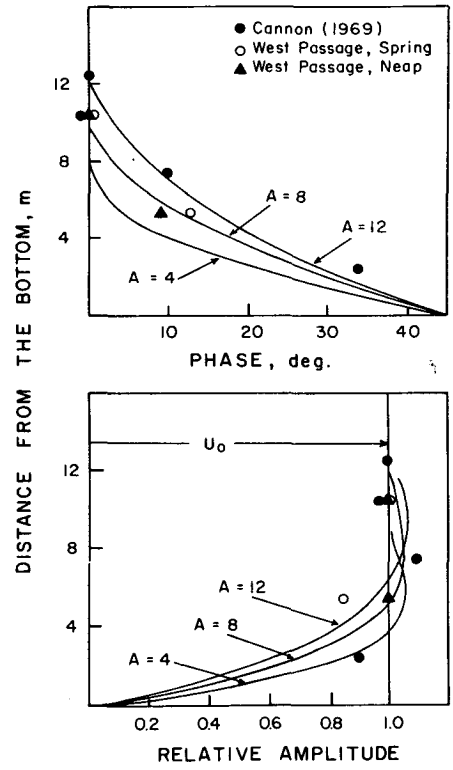

FIG. 10. The vertical distribution of relative amplitude and phase for a simple harmonic oscillation over a flat bottom. Theoretical curves are given for three values of assumed eddy viscosity A. The comparative data points are from Cannon (1969) and the present study.

The transition between wind-dominated estuarine circulation to longer period seasonal variations and the overall response characteristics of estuaries to atmospheric forcing remains an important topic warranting theoretical guidance and further field experimentation.

Acknowledgments. The authors received partial support for this project from the Narragansett Electric Company under University of Rhode Island Grant 98-20-7057, and from the Office of Naval Research under Grant N00014-68-A-0215-0003. We would like to thank Mr. William Kramer for his computer programming assistance.

REFERENCES

Cameron, W. M., and D. W. Pritchard, 1963: Estuaries. *The Sea*, Vol. 2, M. N. Hill, Ed., Wiley, 306–324.

Cannon, G. A., 1969: Observations of motion at intermediate and large scales in a coastal plain estuary. Chesapeake Bay Institute, Tech. Report No. 52.

Hansen, D. V., and M. Rattray, 1965: Gravitational convection in straits and estuaries. *J. Marine Res.*, **23**, 104–122.

——, and ——, 1966: New dimensions in estuary classification. *Limnol. Oceanogr.*, **11**, 319–326.

Hicks, S. D., 1959: The physical oceanography of Narragansett Bay. *Limnol. Oceanogr.*, **4**, 316–327.

——, 1963: Physical oceanographic studies of Narragansett Bay. *U. S. Fish. Wild. Serv., Spec. Sci. Rep. Wild.*, No. 457.

Kowalski, T., *et al.*, 1971: Drifting drogue studies in the vicinity of Rome Point. Rome Point Circulation Study, University of Rhode Island, Tech. Rept. No. 98-20-7057.

Lamb, H., 1932: *Hydrodynamics*. Dover, pp. 738.

Pickard, G. L., and K. Rodgers, 1959: Current measurements in Knight Inlet, British Columbia. *J. Fish. Res. Bd. Can.*, **16**, 635–684.

Pritchard, D. W., and R. E. Kent, 1956: A method for determining mean longitudinal velocities in a coastal plain estuary. *J. Marine Res.*, **15**, 81–91.

Proudman, J., 1953: *Dynamical Oceanography*, Meuthuen and Co. Ltd., 409 pp.

Rattray, M., and D. V. Hansen, 1962: A similarity solution for circulation in an estuary. *J. Marine Res.*, **20**, 121–133.

Sturges, W., 1974: Time scales of deep current during Mode-I. *Mode Hot Line News*, Woods Hole Oceanographic Institution, No. 66.

U. S. Dept. of Commerce, Coast and Geodetic Survey, 1952: *Manual of Harmonic Constant Reductions*. Spec. Publ. No. 260, U. S. Government Printing Office, Washington, D. C.

Weisberg, R. H., and W. Sturges, 1973: The net circulation in the West Passage of Narragansett Bay. Graduate School of Oceanography, University of Rhode Island, Tech. Rept. Ref. No. 3-73, pp. 96.